Simulation of Multi-stage Compressor at Off-Design Conditions

Feng Wang*
Osney Thermo-Fluids Laboratory
Department of Engineering Science
University of Oxford
UK
Email: feng.wang@eng.ox.ac.uk

Mauro Carnevale
Osney Thermo-Fluids Laboratory
Department of Engineering Science
University of Oxford
UK
Email: mauro.carnevale@eng.ox.ac.uk

Luca di Mare
Osney Thermo-Fluids Laboratory
Department of Engineering Science
University of Oxford
UK
Email: luca.dimare@eng.ox.ac.uk

Simon Gallimore
Rolls-Royce plc
Derby
UK
Email: Simon.Gallimore@Rolls-Royce.com

ABSTRACT

Computational Fluid Dynamics (CFD) has been widely used for compressor design, yet the prediction of performance and stage matching for multi-stage, high-speed machines remain challenging. This paper presents the authors' effort to improve the reliability of CFD in multistage compressor simulations. The endwall features (e.g. blade fillet and shape of the platform edge) are meshed with minimal approximations. Turbulence models with linear and non-linear eddy viscosity models are assessed. The non-linear eddy viscosity model predicts a higher production of turbulent kinetic energy in the passages, especially close to the endwall region. This results in a more accurate prediction of the choked mass flow and the shape of total pressure profiles close to the hub. The non-linear viscosity model generally shows an improvement on its linear counterparts based on the comparisons with the rig

*Corresponding author (feng.wang@eng.ox.ac.uk)

data. For geometrical details, truncated fillet leads to thicker boundary layer on the fillet and reduced mass flow and efficiency. Shroud cavities are found to be essential to predict the right blockage and the flow details close to the hub. At the part speed the computations without the shroud cavities fail to predict the major flow features in the passage and this leads to inaccurate predictions of massflow and shapes of the compressor characteristic. The paper demonstrates that an accurate representation of the endwall geometry and an effective turbulence model, together with a good quality and sufficiently refined grid result in a credible prediction of compressor matching and performance with steady state mixing planes.

Introduction

Three-dimensional CFD simulations of multiple blade rows were developed by Adamczyk [1] using the average passage approach. Each blade row was modelled seperately and only one passage of each blade row was required in the simulation. Blade row interactions were evaluated by including additional force terms in the equations. This approach was further simplified by Denton and the resulting approach was termed as the mixing plane approach [2]. The mixing plane assumes a mixed-out state at the bladerow interface by conserving mass, momentum and energy fluxes. The drawback of this approach is that the unsteady blade interactions are removed. Despite its simplicity, the performance of turbomachines is predicted reasonably well using mixing planes. Consequently, steady state RANS simulations have been the work-horse of turbomachinery design. The capability of RANS simulations in assisting turbomachinery design was already demonstrated by early researchers [3, 4], even if limitations in computer power, meshing techniques and physical modelling restricted the spatial resolution as well as the amount of geometric detail present in the simulations.

Typical examples of features omitted from the computational models in the early days were blade fillets, stator shrouds, Variable Stator Vane (VSV) penny gaps etc. Typical grids used were H-grids with pinched tip gaps. Fully meshed tip gaps were introduced and comparisons with pinched tip gaps were summarized by Denton [5]. As the meshing techniques evolved, multiblock structured meshes were introduced into the turbomachinery design and allowed the generation of optimal grids on the blade-to-blade section [6,7]. However, geometrical approximations (e.g. truncated fillets) are still commonplace because of the limitations in the way the geometries of the endwalls and of the blades are represented in the mesh technique.

The effect of endwall geometric features is important in predicting the endwall flows and contributes to setting the flow capacity. One of the most important endwall features for modern machines is the shroud cavities. A typical configuration is shown in Fig. 1. Shabbir et al [8] studied the effect of the hub leakage flow on high speed compressor rotors and the pressure deficit close to the hub was well captured by including the hub leakage flow. Wellborn and Okashi [9] reported the effect of shroud cavities on the performance of multi-stage compressor experimentally. Their data showed that the shroud cavities have considerable negative impact on the compressor performance. In their numerical study, the shroud cavities were not meshed as CFD domains, instead they were introduced through a Knife-to-Knife (K2K) model [10].

Another important element in the construction of steady models for turbomachinery is the turbulence model. The flows in multistage compressor passages are highly viscous and three-dimensional around endwall regions. Furthermore the flow is prone to separation due to strong adverse pressure gradient even at design conditions. Predicting the complex flow features

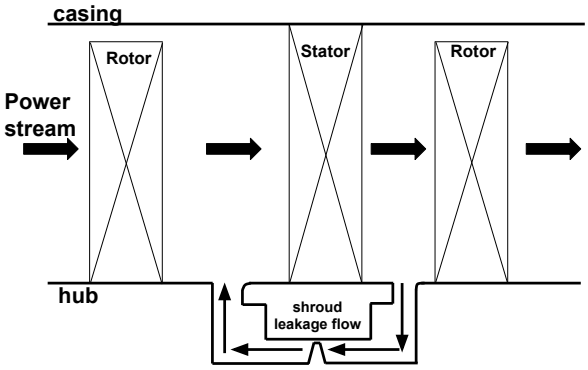

Fig. 1. Schematic of the shrouded compressor.

in a compressor passage with reasonable accuracy poses great challenges to any turbulence model. The turbulence models (e.g. mixing length, Spalart-Allmaras, Wilcox $k-\omega$, SST) used in literature are based the Boussinesq approximation. Recent advances in turbulence modelling introduced an explicit algebraic formulation of the Reynolds stress tensor [11]. This family of turbulence models showed considerable improvement on flows where the flow is against adverse pressure gradient and under mild separations compared to the models such as SST.

Nowadays, computer power, meshing techniques and physical models have progressed greatly with respect to the early days. Finer meshes with more geometrical details become affordable, and larger and larger portions of the flow domain can be fully meshed and included in the computational model [12]. This leaves fewer opportunities to introduce empirical information in the computational model. RANS simulations of multistage compressor are now routinely used in compressor designs. However, reliably predicting the performance and stage matching of high speed machines remains a challenge.

A summary of the challenges faced by numerical analysis was addressed by Denton [5] and Cumpsty [13]. The strategy proposed by Denton and Cumpsty is to eliminate or minimize the errors or uncertainties in the boundary conditions and geometry, and improve the fidelity of physical modelling. There is a need for a systematic appraisal of the effect of geometrical features, modelling level and turbulence model within the framework of steady state RANS for multistage compressor CFD. This study presents such a systematic appraisal by studying an 8-stage compressor.

Methodology

CFD Solver

The CFD simulations in this paper are performed with the in-house CFD solver AU3X [14]. AU3X solves the unsteady Reynolds Averaged Navier-Stokes equations using a fully implicit cell-centred finite volume scheme on unstructured or structured meshes. The flow gradients are evaluated with the weighted least-square method. Inviscid fluxes are computed by Roe's Riemann solver. Second-order accuracy in space discretization is achieved by the Monotonic Upstream-Centered Scheme for Conservation Laws (MUSCL) approach with the van Albada limiter. Steady and unsteady solutions are obtained via pseudo time-marching and dual-time stepping respectively. A list of popular turbulence modes are available in the solver. In this study, the ω-based two-equation models are examined, namely Wilcox $k-\omega$ [15], Menter Shear Stress Transport (SST) [16] and an Explicit Algebraic Reynolds Stress Model (EARSM) which was recently proposed by Menter [11]. The

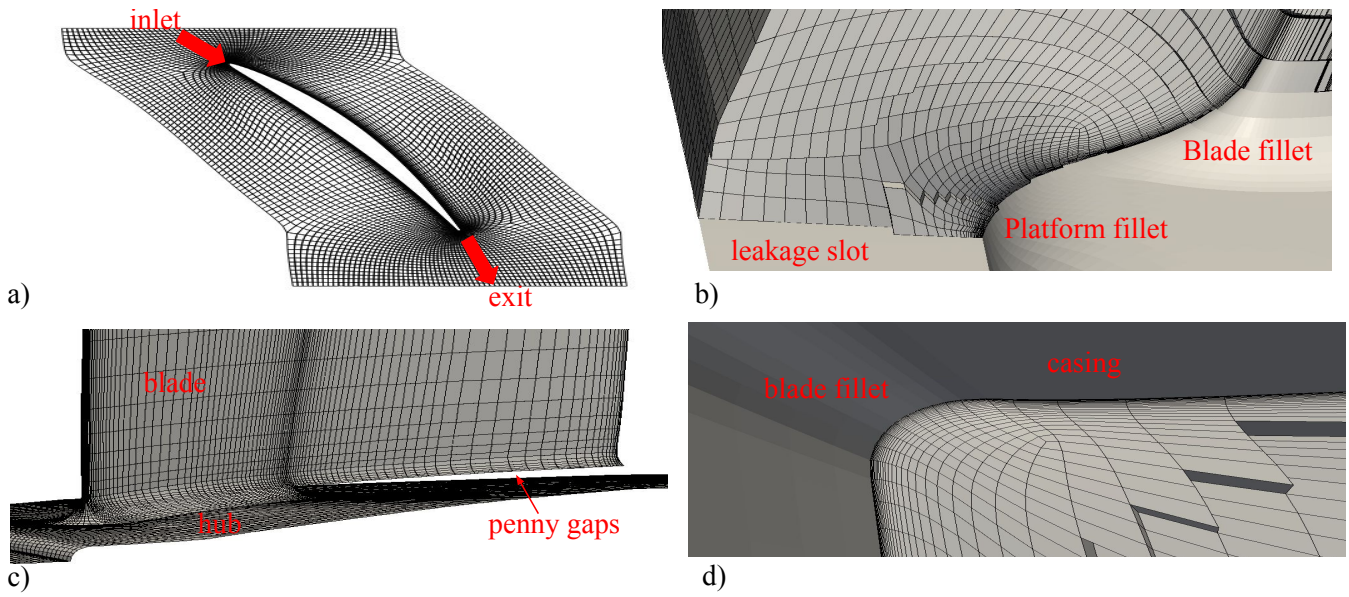

Fig. 2. a): Mesh on the blade-to-blade section. b): Close-up view of the mesh around the platform fillet. c): Mesh for a stator variable vane with penny gaps. d): Boundary layer mesh around the blade fillet. The figures have been intentionally distorted.

air is assumed to be perfect gas and its viscosity is evaluated with Sutherland's law to take into account the large temperature variation across the compressor. The solver has been validated extensively on the compression system [17, 18] and recently the solver has been optimised in modern multicore and manycore architectures and the details are reported by Hadade and di Mare [19].

Mesh Generation

Hexahedral meshes for blade passages are generated using an in-house multi-block structured mesh generator developed by Wang [20]. The mesh generator builds fully 3D blocks in the blade passage. The exact tangency condition between the blade fillet and endwalls is not compromised and the shape of the platform edges can be meshed with no approximations and optimal mesh quality.

The meshing algorithm generates an algebraic mesh in the first place and then smooths it by solving a system of 3D elliptic equations. Sources are computed on the viscous wall boundaries to control the grid spacing and grid orthogonality close to the wall. Figure 2 shows the typical meshes used in this study. The blade leading edges of middle and rear stages in shrouded compressors are typically close to the platform (see Fig. 2 b)). The current mainstream method to mesh turbomachinery blade passages is essentially to sweep a mesh from the hub to the casing. This method has to truncate the fillets and platforms. In the case of the scenario in Fig. 2 b), the fillet at the leading edge meets the hub at an angle of roughly 180°. This will generate extremely distorted cells around the platform leading edge region.

The meshes for the shroud cavities are generated using an in-house hybrid mesh generator developed by Wang and di Mare [21]. Boundary layer meshes are generated close to the viscous walls and triangles are used to fill the rest of the domain. Collisions of boundary layer meshes are detected by geometry reasoning using the Constrained Delaunay Triangulation (CDT). Figure 3 shows a typical hybrid mesh for a stator shroud cavity.

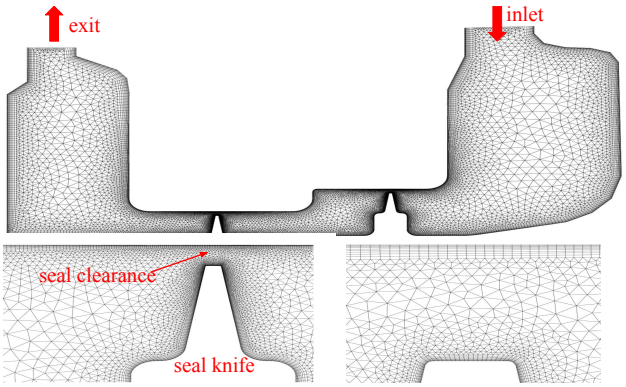

Fig. 3. Hybrid mesh for the shroud cavity under S4. The figure has been intentionally distorted.

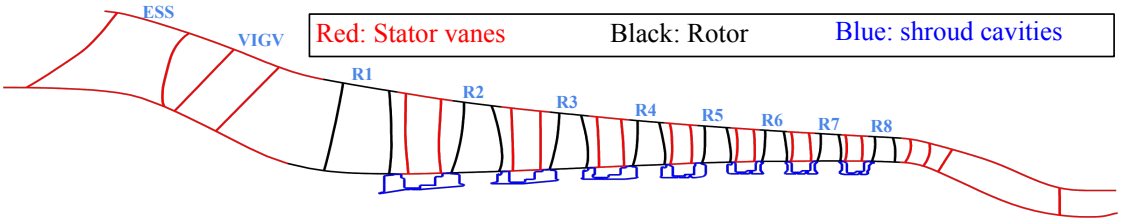

Fig. 4. Schematic of the compressor model. The figure has been intentionally distorted.

Results and Discussion

This section is organized as the following. The rig and the computational model are described in the first place. The results on the 100% speed are presented. These include the grid sensitivity study, the effects of turbulence model and endwall geometry. The results on the 85% speed are then reported.

Case Study

The compressor studied in this paper is representative of a modern high speed machine. The compressor has 8 stages with shrouded stators. A row of Engine Section Stators (ESS) and a row of Variable Inlet Guide Vanes (VIGV) are placed upstream of Rotor 1 (R1). A row of large struts are placed downstream of the last stator blade-row (S8). The stators of stages 1 and 2 are also variable and, together with the VIGV row, are used to control the machine at part-speed. The stator of stage 3 also has provisions to modify its stagger, and features penny gaps at the hub and casing, but its setting is not modified during tests. The leading edges of selected stator vanes are instrumented for performance measurements. Tip and penny gap clearances are set to their nominal values. Stator hub shrouds for S1 to S7 are fully meshed and included in the model but the hub leakage upstream of R1 is not included. The nominal fin clearance is used for all the stator shroud seals.

A schematic view of the CFD model is shown in Fig. 4. The stators are coloured in red, the rotors are coloured in black and the shroud cavities are in blue. The blade counts in the ESS and VIGV blade-rows are identical. This allows a sliding plane to be placed between them to enable the wake of the ESS to enter the VIGV passage. Mixing planes are used on all remaining blade-blade and blade-cavity interfaces.

Design Speed

Grid Sensitivity Study

Grid sensitivity study is not conducted on the whole compressor. Instead it is done separately on the blade passages and the shroud cavities at the design speed. The study on the blade passage is conducted on the block which constrains the stability limit of the whole compressor. The mesh resolution from this study provides guidelines on other blade rows. The study on the shroud cavity is performed on the shroud cavity of stage 4 and the mesh resolution of this cavity is taken as the guidelines for other shroud cavities.

For the blade passage, two studies are undertaken. In the first study, only fillets and penny gaps are included among the endwall features. In the second study, the shroud slots are included and the boundary conditions of the slots are taken from simulations of the whole compressor with shroud cavities included.

The study on the passage grid is performed on bladerows S3, R4 and S4. This choice is motivated by the fact that the stability limit of this compressor is set by these blade rows. Two sets of grids are generated. The first one (Medium) has around 0.9 million cells for each blade row and the second one (Fine) has around 1.8 million cells for each blade row. Tip and penny gaps are meshed with 20 and 30 layers of grid cells for the two grids, respectively. Both meshes have an average $y^+ \approx 1$ on the blade and endwall. The mesh refinement is conducted in an approximately isotropic fashion, so that the Fine and Medium grid cells have approximately the same aspect ratio distribution. The expansion ratio of the boundary layer grids in the Fine grid is reduced compared to the expansion ratio in the Medium grid from roughly 1.2 to 1.1. The EARSM turbulence model is used in the grid sensitivity study.

The convergence of the simulations is judged by monitoring the primary performance parameters (e.g. massflow and total pressure) and the residuals of the mass flux, momentum flux, energy flux and fluxes for turbulent variables for each bladerow or cavity. At off-design conditions where flow separation occurs, the residuals might oscillate and the primary performance parameters are given more weight on the judgement of convergence. This strategy is used for all the simulations in this paper.

The pressure ratio and efficiency are evaluated at the planes upstream of the leading edges of S3 and S4. The axial position of the plane is 5% of the axial chord upstream the leading edge in the middle span. If not stated explicitly, the mass-averaged data (e.g. total pressure, total temperature and flow angles) for other stator rows are evaluated in the same strategy. The computed pressure ratio and efficiency for S3-S4 block is shown in Fig.5. The two meshes yield almost identical results at the design point and only minor deviations are seen at higher working lines. Therefore by doubling the mesh sizes, the predicted performance for the S3-S4 block changes marginally.

The passage grid study with shroud slots is performed to understand the effect of mesh resolution on the flow leaving the shroud slot ahead of the stator leading edges (see Fig. 2 b)). This study is conducted on S3 and the boundary conditions are extracted from a whole compressor simulation at the design point. Computations are performed on two grids. The first grid uses the meshing parameters of the medium grid in the previous study. The second grid retains all the meshing parameters but doubling the mesh size of the block on the platform fillet. The radial flow angles in front of the leading edge is shown Fig. 6. The difference of the radial flow angle between the medium and the fine mesh is less than 0.05°. The mesh size of

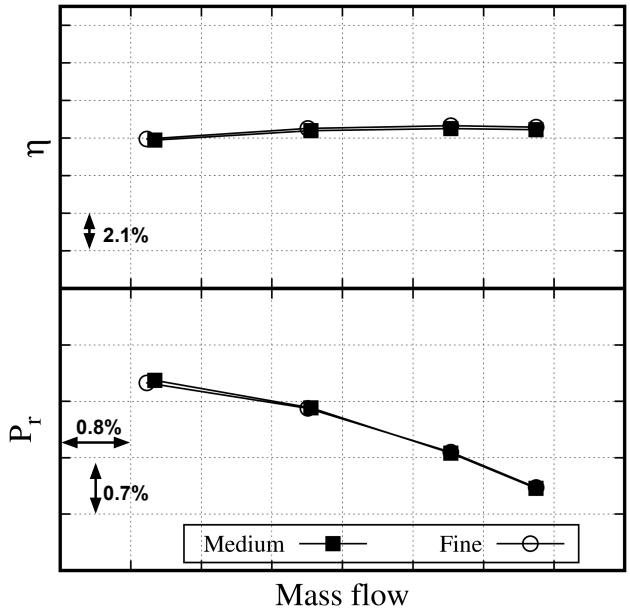

Fig. 5. Grid sensitivity study of S3-S4 block.

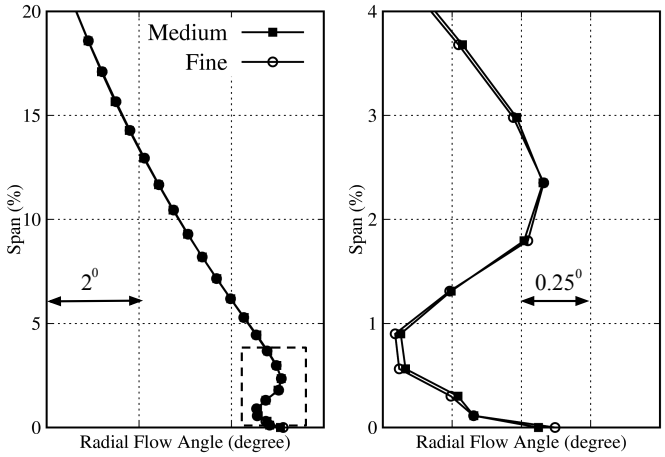

Fig. 6. Radial flow angle in front of S3 leading edge with two sets of meshes. Left: radial flow angles within 20% span. Right: radial flow angles within 4% span.

the medium mesh on the platform fillet is adequate for predicting the effect of shroud leakage flows.

Therefore the meshing parameters for the medium grid in the previous studies are used to mesh the blade passages. The average cells in each passage is around 0.9 million and y^+ is approximately 1 on the blade and endwall.

The shroud cavity of S4 in the middle stage is chosen for the grid dependence study on shroud cavities. Three levels of hybrid meshes are generated. The number of quadrilateral inside the boundary layer mesh and triangles away from the wall are detailed in the Table 1. All the mass flows are normalised by the mass flow resulting from the use of the finest mesh. By refining the mesh from the coarse to the medium level, the relative difference is 2.27% and further refinement leads to a relative difference of 0.28%. Since the mass flow in the shroud cavity is normally two orders of magnitude smaller than the mass flow in the mainstream, the difference of the mass flow computed by the medium mesh and the fine mesh is negligible. The mesh with the medium size is then used for all the shroud cavities.

Table 1. Grid sensitivity study of shroud cavity

	Quad.	Tri.	Normalised Massflow
Coarse	17387	26894	1.0228
Medium	40049	588226	1.0028
Fine	66910	706700	1.0000

Table 2. Summary of Model setups.

Setup	Turb.	Fillets	Penny gaps	Shroud cavity
0	EARSM	✓	X	X
1	Wilcox $k-\omega$	✓	✓	X
2	Menter SST	✓	✓	X
3	EARSM	✓	✓	X
4	Menter SST	✓	✓	✓
5	EARSM	✓	✓	✓

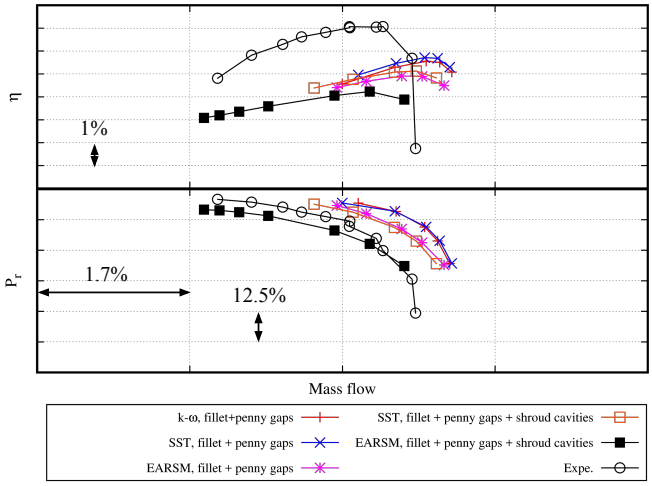

Fig. 7. Compressor map using different turbulence models and geometry details at the 100% speed. Data are normalised by their corresponding values at the design point of the 100% speed.

Effect of Turbulence Models

The effect of turbulence models is first studied without including the shroud cavities. This study is shown as setup 1-3 respectively in Table 2. As is shown in Fig. 7, $k-\omega$ and SST predict similar overall performances of the compressor and the shape of the experimental pressure rise characteristic is captured reasonably well by both models. Discrepancies are only observed at high working line conditions. This can be explained by the formulations (see Equation 1) of eddy viscosity in both turbulence models. a_1 is a constant and SF_2 is a term related to the local strain rate.

$$\nu_t = \begin{cases} \frac{k}{\omega} & k-\omega \\ \frac{a_1 k}{max(a_1\omega, SF_2)} & \text{SST} \end{cases} \quad (1)$$

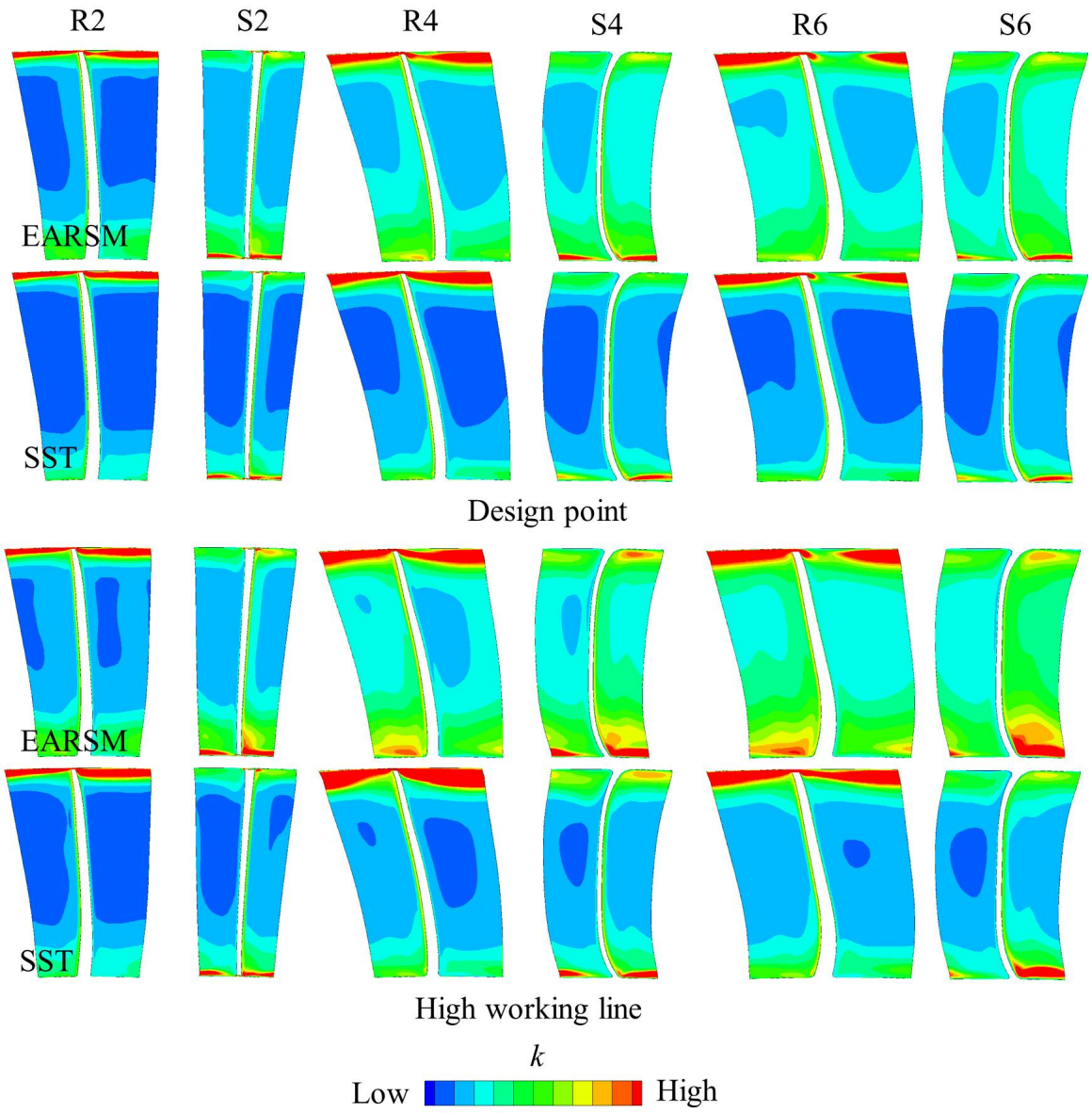

Fig. 8. Turbulent kinetic energy on the mid-chord plane at the design and high working line conditions of the 100% speed. The figures have been intentionally distorted.

In most of the adverse pressure regions, the eddy viscosity of SST is computed as $\frac{a_1 k}{SF_2}$. Otherwise it has the same formulation of the eddy viscosity as $k-\omega$. When the flow encounters stronger pressure gradient at high working line conditions, the term $\frac{a_1 k}{SF_2}$ becomes more active and results in the differences observed in Fig. 7. The mass flow predicted by EARSM is closer to the experimental curve and the shape is also better captured compared to the previous two. However, a lower efficiency is predicted by EARSM. A similar trend can also be observed for simulations (setup 4 and 5) where shroud cavities are included.

The difference between $k-\omega$ or SST and EARSM is mainly due to the way the Reynolds stress tensor is evaluated. The evaluation of the Reynolds stress tensor in $k-\omega$ or SST is based on the Boussinesq eddy viscosity assumption. In EARSM

the Boussinesq assumption is no longer used and the Reynolds stress tensor is evaluated according to

$$\overline{-\rho u_i' u_j'} = -\rho k(a_{ij} + \frac{2}{3}\delta_{ij}) \tag{2}$$

$$a_{ij} = \beta_1 \sigma_{1,ij} + \beta_2 \sigma_{2,ij} + \cdots + \beta_9 \sigma_{9,ij} \tag{3}$$

The Reynolds stress tensor is expanded as a polynomial. The basis and coefficients of the polynomial are all functions of the mean flow gradients. The evaluation of the Reynolds stress tensor of the $k-\omega$ or SST model can be considered as an approximation of the first order term in Equation 2. The effects of the high order terms can be demonstrated by plotting k of SST and EARSM at design and high working line conditions for setup 4 and setup 5, as shown in Fig. 8. The following observations can be made:

1. k is higher around mid-span regions in the EARSM solutions at both design and high working line conditions. The differences between both models are gradually accumulated across the machine. This is because EARSM produces higher k for each blade row and k is conserved through the mixing plane. The extra k is passed downstream and this effect gradually builds up across the stages.
2. The most pronounced difference is observed around the hub region for both rotors and stators, where EARSM produces higher k compared to SST. This enhances the momentum transfer around the hub region and results in stronger secondary flows.
3. The extra k in the EARSM solution is generated by the higher order terms in Equation 2. This demonstrates that the high order terms plays an important role in the production of k and prediction of the flow fields, especially around the endwall regions.

In terms of block performance and stage matching (see Fig. 9), the solutions of $k-\omega$ and SST under-predict the pressure ratio in the front stage due to the over-prediction of the inlet mass flow. Since the total pressure ratio is constrained by the boundary conditions, the pressure ratio of the rear stage is over-predicted. For the EARSM solution, it predicts a more accurate massflow and this results in a better stage matching.

Effect of Endwall Features

Typical endwall features include blade fillets, penny gaps and shroud leakage slots. The blade fillet is normally approximated due to the limitation of the conventional meshing technique, which generates the 3D meshes by sweeping a mesh from the hub to the casing. The blade fillet has to be truncated to avoid generating distorted cells around the region where the fillet meet the endwalls. The effect of the truncated fillet on the predicted compressor performance map is shown in Fig. 10. Setup 0 in Table 2 is used in this study. The simulations with the truncated fillet has a truncation angle of 45° and the mesh sizes are comparable to the medium mesh in the grid sensitivity study. No penny gaps and shroud cavities are included. Therefore the difference in the prediction of the compressor map is due to the truncation of the blade fillets.

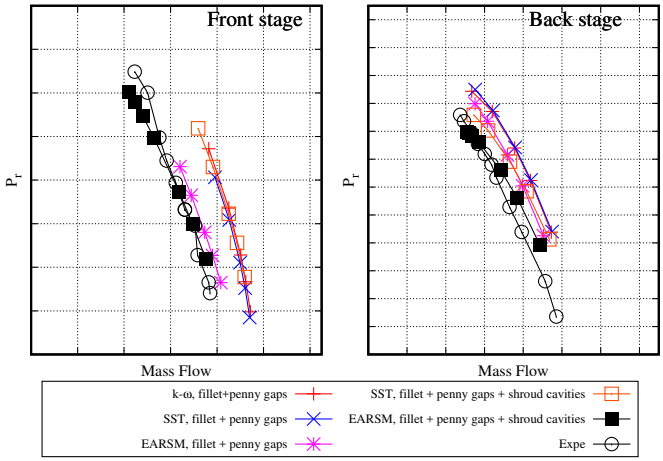

Fig. 9. Stage performance for the front stage and one of the back stages.

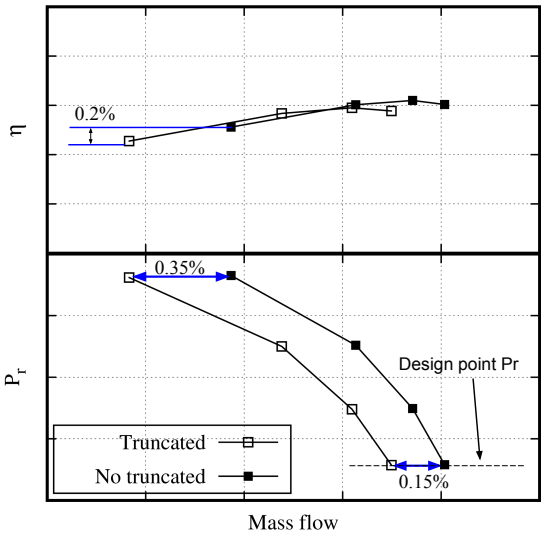

Fig. 10. Compressor map computed by meshes with truncated and non-truncated fillets at the 100% speed. Values are normalised by the choked massflow of the experiment.

It can be clearly seen that the simulation with truncated fillet predicts a massflow which is 0.15% lower than the one without truncating the fillet at the design point. This difference increases gradually to 0.3% at the high working line condition. For multi-stage compressors, the difference of 0.3% in inlet massflow is by no means a negligible value and it could result a re-matching of the compressor if allowed to accumulate blade-row after blade-row. In terms of efficiency, the difference at the design point is small but it increases to 0.2% at the high working line condition.

The difference observed in Fig. 10 can be demonstrated by a close-up view of the flow fields around the fillet. Figure 11 shows the Mach number distribution around the fillet at the mid-chord plane of S3 at the design point. The truncation generates a spurious corner feature around this region. In turn, this generates an artificial flow feature and results in a thicker boundary layer on the fillet. Figure 12 shows the distribution of total pressure coefficient at the exit of S3. The thickened boundary layer on the fillet contributes to the endwall blockage, yields stronger wakes and extra losses. Therefore it is noted that a non-truncated fillet should be used for multistage compressor simulations to minimize the errors caused by geometrical approximations.

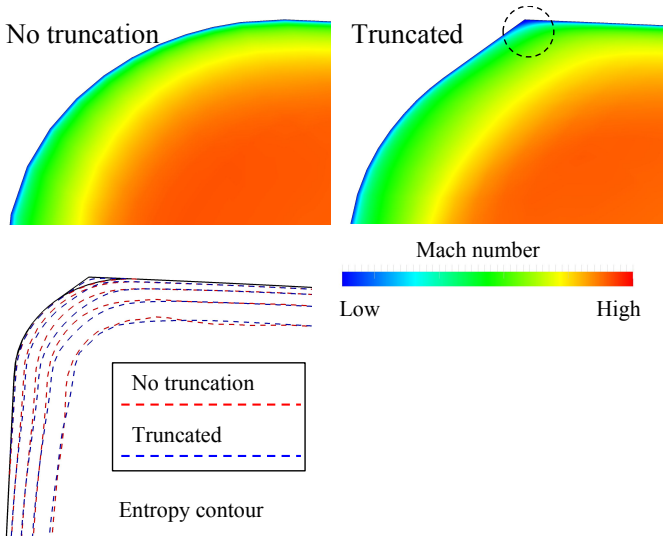

Fig. 11. Comparison of truncated and non-truncated fillet - I.

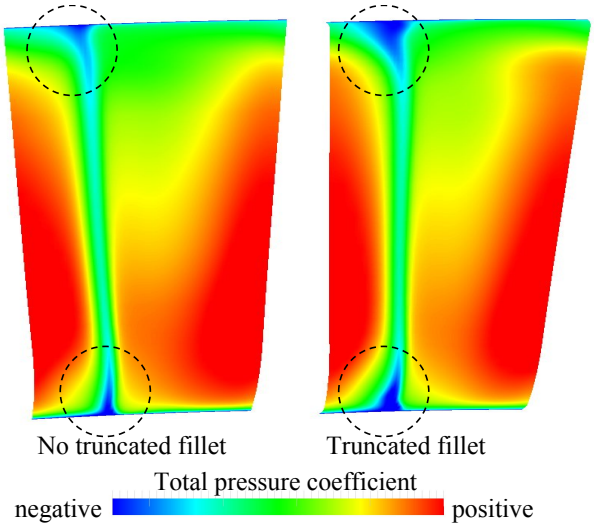

Fig. 12. Comparison of truncated and non-truncated fillet - II. The figure has been intentionally distorted.

The above study shows the effect of the truncated fillet using the conventional meshing technique. Similarly, when shroud cavities are included, the platform leading edge may also need to be truncated. For mechanical reasons, the platform leading edge also has a fillet (see Fig. 2 b)). When the blade leading edge is too close to the platform leading edge, the conventional technique which truncates the blade fillet and the platform leading edge fillet will fail to produce a mesh with acceptable quality, unless the geometry is modified so that the blade leading edge is sufficiently far away from the platform. This difficulty is overcome by the meshing technique used in the current study. The simulations with shroud cavities in this study have minimal approximations of the platform shape. The SST and EARSM models are used to compute the compressor performance (setup 4 and 5) and the results are shown in Fig. 7.

The solutions with shroud cavities yield reduced massflow and efficiency and the curves of the pressure ratio become less steep. Furthermore, the solutions with EARSM covers the whole operating range of the compressor and the stall margin is predicted remarkably well. The reduction of the mass flow and efficiency is due to the purge air entering the power stream

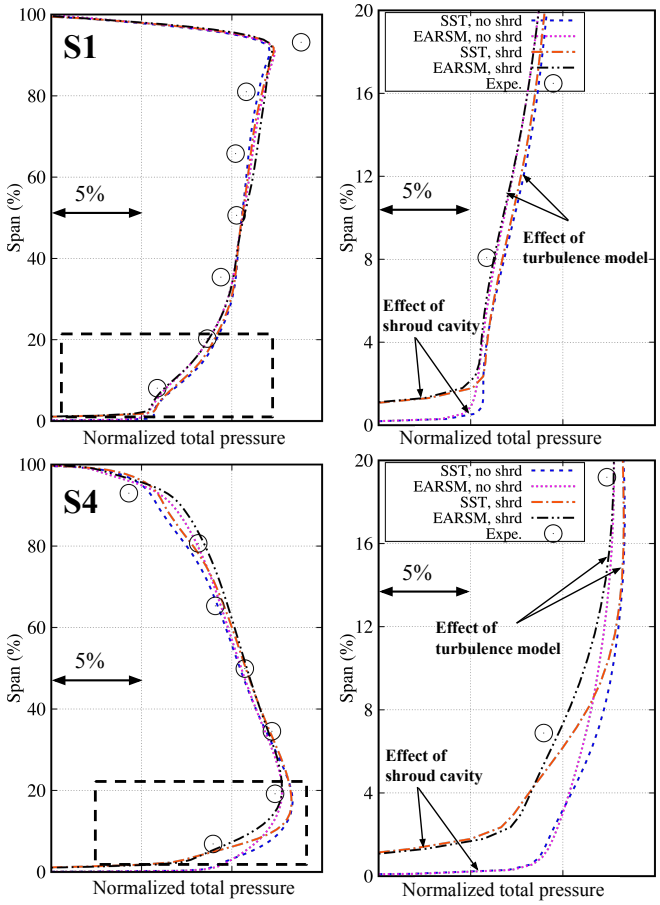

Fig. 13. Comparison of total pressure radial profiles in front of S1 and S4 leading edges.

from the shroud cavities in front of the stators. This effect can be demonstrated by the radial profile of total pressure in front of S1 and S4 at a high working line condition. By adding shroud cavities, more losses are introduced close to the hub and this results in better matching with the experimental data. Furthermore, for both turbulence models, Figure 13 shows that adding shroud cavities only modifies the flow field immediately close to the hub. The flow away from the hub is less sensitive to the effect of shroud cavities but is sensitive to the turbulence models.

In terms of block performance and stage matching (see Fig. 9), the mass flow is further reduced by adding the shroud cavity. This increases the pressure ratio of the front stage and reduces the pressure ratio of the rear stage for the solutions of SST and EARSM. It can be observed that the stage matching is improved by including the shroud cavities.

Part Speed

The study in the 100% speed demonstrates the effects of turbulence models and endwall features. At the 85% speed, only the EARSM model is used and the effect of shroud cavities is studied.

The computed compressor performance at part speed is shown in Fig. 14. Two sets of simulations are prepared, one with shroud cavities and the other one without shroud cavities. For the simulations with shroud cavities, the massflow is predicted very accurately and the stall margin is predicted reasonably well. The shape of the experimental curves for both pressure ratio and efficiency is well captured but the efficiency is marginally under-predicted. Without the shroud cavities,

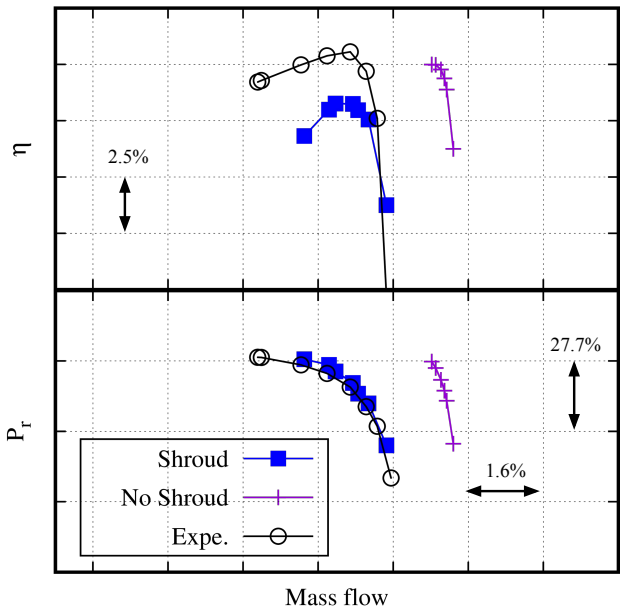

Fig. 14. Compressor map at the 85% speed. Data are normalised by their corresponding values at the design point of the 85% speed.

the massflow is considerably overpredicted. The pressure rise characteristic is too steep and the predicted efficiency does not show the gradual reduction of efficiency after the peak efficiency seen in the measurements.

The difference observed in the compressor characteristic can be best demonstrated by the flow fields at S1 and R2. Figure 15 shows the distribution of total pressure coefficient on the S1 and R2 mid-chord planes at the design point of the 85% speed. The distribution of total pressure coefficient is very similar for both simulations towards the casing, however, the simulation without the shroud cavity ignores the effect of the leakage air. The leakage air enters the power stream and loses total pressure when it encounters the separation region at the leading edge due to turbulent mixing. As the leakage air travels downstream, it cannot overcome the adverse pressure gradient in the power stream and leads to flow separation [8]. Therefore the simulation without the shroud cavities significantly underpredicts the hub separation at S1 and then fails to predict the corner stall at the downstream R2. This is demonstrated in Fig. 15.

In terms of radial profiles, the profiles of the total pressure in front of the leading edges of S1 and S2 are shown in Fig. 16. The effect of the shroud cavity for S1 is only observed close to the hub and this is similar to the observation in the 100% speed. A major feature in the profile of S2 is the dip around the 20% span. This indicates significant loss production at the upstream R2. Without the shroud cavities, this flow feature is not captured by the simulations. This is because the total pressure deficit around the 20% span is caused by the corner stall of the upstream R2 (see Fig. 15) and this is missed by the simulations without shroud cavities. With the shroud cavities included, this flow feature is captured remarkably well.

Conclusions

This paper presents simulations of an 8-stage shrouded, high speed axial compressor using steady state RANS. The objective of the paper is to examine the effect of turbulence models and endwall features on the prediction of the compressor performance. The paper also shows that an accurate representation of the endwall geometry and an effective turbulence

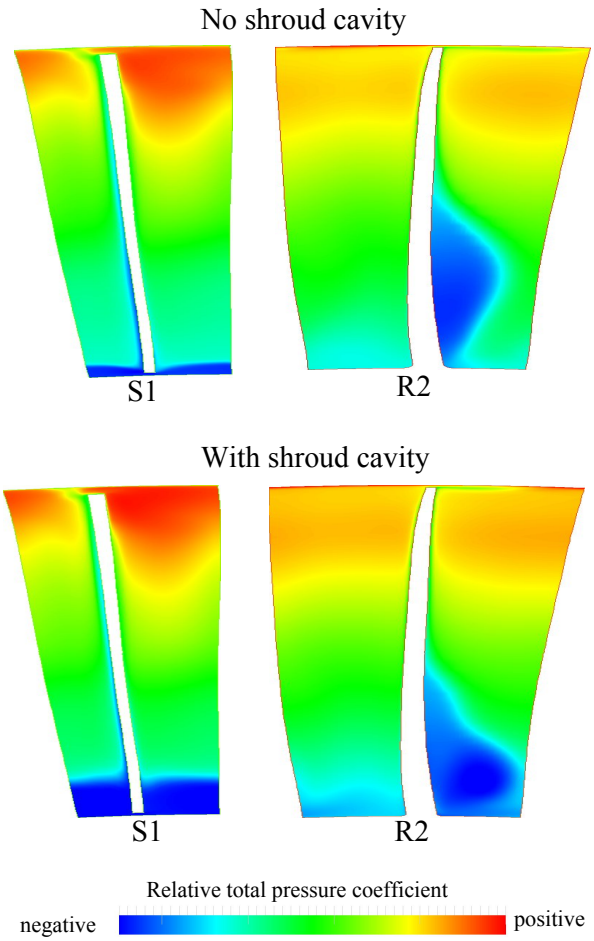

Fig. 15. Relative total pressure coefficient at the mid-chord plane of S1 and R2 at the design point of the 85% speed. This figure has been intentionally distorted.

model, together with a good quality and sufficiently refined grid result in credible predictions of the performance with steady state mixing planes both at design speed and at part speed.

Shroud cavities are found to be essential to capture the flow features towards the hub at both design and part speeds. It has also been shown that the capability of existing meshing techniques and turbulence models is such that empirical models can be confidently replaced by CFD calculations for these components. The direct effect of the shroud cavities at the design speed is confined close to the hub but this effect is more pronounced at part speed. The simulations without the shroud cavities at part speed under-predict the flow separation at S1 hub and this leads to a failure in predicting the hub corner stall at R2. Because of this, the shape of the radial profiles of total pressure at S2 leading edge is inaccurately predicted.

ω-based two-equation turbulence models are assessed. For the simulations without shroud cavities $k-\omega$ and SST generate similar solutions at the design point and minor differences are only observed at the high working line. EARSM generally yields an improvement over the previous two models. The high order terms in the formulation of the Reynolds stress tensor in EARSM are found to be play an important role and lead to larger values of k in the blade passages. This yields a realistic level of mixing and blockage in comparison to the experimental data. The shape of the radial profiles of total pressure is largely determined by the choice of turbulence models. Adding shroud cavities only modifies the shapes

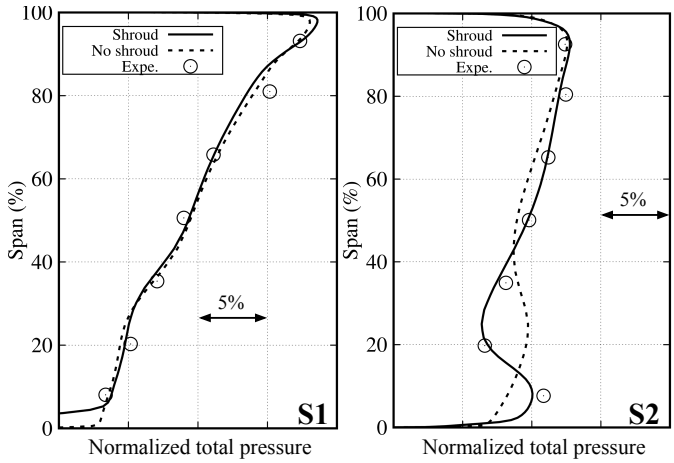

Fig. 16. Radial profiles of total pressure in front of S2 leading edge at the design point of the 85% speed.

close to the hub.

For the 100% speed, the choked mass flow is predicted accurately. The full operating range of the compressor in terms of mass flow is covered and the stall margin is predicted remarkably well. For the 85% speed, the massflow is predicted satisfactorily and the radial profiles also match very well with the experimental data.

Acknowledgements

The authors are grateful to Rolls-Royce plc for funding this work under the SIMulation Off-Design (SIMOD) project (Innovate UK grant 101288) and granting permission for its publication.

Nomenclature

a_1 Constant in the formulation of eddy viscosity in SST model, [-]

k Turbulent kinetic energy, $[m^2/s^2]$

M Normalised mass flow, [-]

P_0 Total pressure, [Pa]

P_{av} Mass averaged total pressure, [Pa]

Pr Total-to-total pressure ratio, [-]

β Coefficient of the polynomial of Reynolds stress tensor in EARSM, [-]

η Adiabatic efficiency, [-]

ν_t Turbulent eddy viscosity, [kg/(ms)]

σ Base of the polynomial of Reynolds stress tensor in EARSM, [-]

ω Specific dissipation rate, $[s^{-1}]$

References

[1] Adamczyk, J., 1984. Model equation for simulating flows in multistage turbomachinery. Technical Report NASA-TM-86869, NASA, NASA Lewis Research Center, Cleveland, USA.

[2] Denton, J. D., 1992. "The calculation of three-dimensional viscous flow through multistage turbomachines". *Journal of Turbomachinery,* ***114***(1), pp. 18–26.

[3] Denton, J., and Dawes, W., 1998. "Computational fluid dynamics for turbomachinery design". *Proceedings of the Institution of Mechanical Engineers, Part C: Journal of Mechanical Engineering Science,* ***213***, pp. 107–124.

[4] Gallimore, S. J., Bolger, J. J., Cumpsty, N. A., Taylor, M. J., Wright, P. I., and Place, J. M., 2001. "The use of sweep and dihedral in multistage axial flow compressor blading-part I: University research and methods development". *Journal of Turbomachinery,* ***124***(4), pp. 521–532.

[5] Denton, J., 2010. "Some limitations of turbomachinery CFD". In Proceedings of ASME Turbo Expo 2010: Power for Land and Sea and Air, no. GT2010-22540, pp. 735–745. June, Glasgow,UK.

[6] Shahpar, S., and Lapworth, L., 2003. "PADRAM: Parametric design and rapid meshing system for turbomachinery optimisation". In Proceedings of ASME Turbo Expo 2003, no. GT2003-38698, pp. 579–590. June, Atlanta, USA.

[7] Wang, F., 2013. "Whole aero-engine meshing and CFD simulation". PhD thesis, Imperial College London.

[8] Shabbir, A., Celestina, M., Adamczyk, J., and Strazisar, A., 1997. "The effect of hub leakage flow on two high speed axial flow compressor rotors". In Proceedings of ASME 1997 International Gas Turbine and Aeroengine Congress and Exhibition, no. GT-346. June, Orlando, USA.

[9] Wellborn, S., and Okiishi, T., 1999. "The influence of shrouded stator cavity flow on multistage compressor performance". *Journal of Turbomachinery,* ***121***, pp. 486–497.

[10] Wellborn, S. R., Tolchinsky, I., and Okiishi, T., 1999. "Modeling shrouded stator cavity flows in axial-flow compressors". *Journal of Turbomachinery,* ***122***(1), pp. 55–61.

[11] Menter, F., Garbaruk, A., and Egorov, Y., 2012. "Explicit algebraic reynolds stress models for anisotropic wall-bounded flows". *Progress in Flight Physics,* ***3***, pp. 89–104.

[12] Wang, F., Carnevale, M., Lu, G., di Mare, L., and Kulkarni, D., 2016. "Virtual gas turbine: Pre-processing and numerical simulations". In Proceedings of ASME Turbo Expo 2016, no. GT2016-56227. Seoul, South Korea.

[13] Cumpsty, N., 2010. "Some lessons learned". *Journal of Turbomachinery,* ***132***(4), pp. 1–7.

[14] di Mare, L., Kulkarni, D. Y., Wang, F., Romanov, A., Ramar, P. R., and Zachariadis, Z. I., 2011. "Virtual gas turbine: Geometry and conceptual description". In Proceedings of ASME Turbo Expo 2011, no. GT2011-46437, pp. 347–358. June, Vancouver, Canada.

[15] Wilcox, D. C., 1988. "Reassessment of the scale-determining equation for advanced turbulence models". *AIAA Journal,* ***26***(11), pp. 1299–1310.

[16] Menter, F., 1994. "Two-equation eddy-viscosity turbulence models for engineering applications". *AIAA Journal,* ***32***(8), pp. 1598–1605.

[17] Carnevale, M., Wang, F., Green, J., and Mare, L., 2015. "Lip stall suppression in powered intakes". *Journal of*

Propulsion and Power, ***32***(1), pp. 161–170.

[18] Carnevale, M., Wang, F., and di Mare, L., 2017. "Low frequency distortion in civil aero-engine intake". *Journal of Engineering for Gas Turbines and Power,* ***139***(4), p. 041203.

[19] Hadade, I., and di Mare, L., 2016. "Modern multicore and manycore architectures: Modelling, optimisation and benchmarking a multiblock CFD code". *Computer Physics Communications,* ***205***(Supplement C), pp. 32 – 47.

[20] Wang, F., and di Mare, L., 2017. "Mesh generation for turbomachinery blade passages with three-dimensional endwall features". *Journal of Propulsion and Power*. https://doi.org/10.2514/1.B36356.

[21] Wang, F., and di Mare, L., 2016. "Hybrid meshing using constrained delaunay triangulation for viscous flow simulations". *International Journal for Numerical Methods in Engineering,* ***108***(13), pp. 1667–1685.